

$Y_xAl_{1-x}N$ Thin Films

Agnė Žukauskaitė, Christopher Tholander, Justinas Pališaitis, Per O. Å. Persson,
Vanya Darakchieva, Nebiha Ben Sedrine, Ferenc Tasnádi, Björn Alling,
Jens Birch and Lars Hultman

Linköping University Post Print

N.B.: When citing this work, cite the original article.

Original Publication:

Agnė Žukauskaitė, Christopher Tholander, Justinas Pališaitis, Per O. Å. Persson, Vanya Darakchieva, Nebiha Ben Sedrine, Ferenc Tasnádi, Björn Alling, Jens Birch and Lars Hultman, $Y_xAl_{1-x}N$ Thin Films, 2012, Journal of Physics D: Applied Physics, (45), 42, 422001.

<http://dx.doi.org/10.1088/0022-3727/45/42/422001>

Copyright: Institute of Physics

<http://www.iop.org/>

Postprint available at: Linköping University Electronic Press

<http://urn.kb.se/resolve?urn=urn:nbn:se:liu:diva-76472>

$Y_xAl_{1-x}N$ thin films

Agnė Žukauskaitė^{1*}, Christopher Tholander¹, Justinas Palisaitis¹, Per O. Å. Persson¹, Vanya Darakchieva², Nebiha Ben Sedrine^{2,3}, Ferenc Tasnádi⁴, Björn Alling¹, Jens Birch¹ and Lars Hultman¹

¹ Thin Film Physics Division, Department of Physics, Chemistry, and Biology (IFM), Linköping University, SE-581 83 Linköping, Sweden.

² Semiconductor Materials Division, Department of Physics, Chemistry, and Biology (IFM), Linköping University, SE-581 83 Linköping, Sweden.

³ IST/ITN Instituto Superior Técnico, Universidade Técnica de Lisboa, 2686-953 Sacavém, Portugal

⁴ Theoretical Physics Division, Department of Physics, Chemistry, and Biology (IFM), Linköping University, SE-581 83 Linköping, Sweden.

E-mail: agne@ifm.liu.se

Abstract. Reactive magnetron sputtering was used to deposit $Y_xAl_{1-x}N$ thin films, $0 \leq x \leq 0.22$, onto $Al_2O_3(0001)$ and $Si(100)$ substrates. X-ray diffraction and analytical electron microscopy show that the films are solid solutions. Lattice constants are increasing with Y concentration, in agreement with *ab initio* calculations. Spectroscopic ellipsometry measurements reveal a band gap decrease from 6.2 eV ($x=0$) down to 4.5 eV ($x=0.22$). Theoretical investigations within the special quasirandom structure approach show that the wurtzite structure has the lowest mixing enthalpy for $0 \leq x \leq 0.75$.

PACS 81.15.Cd, 78.20.-e, 64.60.My, 77.84.Bw, 31.15.A-

Submitted to Journal of Physics D: Applied physics

I. Introduction

In the view of recent interest of alloying group IIIA and IIIB nitrides we present a study on AlN-rich $Y_xAl_{1-x}N$ thin films. Previous reports on this compound are limited to YN-rich bulk Y-Al-N [1]. AlN

* Corresponding author. agne@ifm.liu.se

has a hexagonal wurtzite structure and is a wide band gap (6.2 eV) piezoelectric polar material with various electroacoustic and optoelectronic applications such as piezoelectric active layer in thin-film bulk-acoustic resonator structures (TFBARs). It is chemically and high-temperature stable, and is known for its low acoustic losses, high Q values as well as the highest piezoelectric constant ($e_{33}=1.46 \text{ C/m}^2$) among group III nitride semiconductors [2]. Recently, studies on alloying AlN with ScN reported a significant increase in the piezoelectric response and electromechanical coupling [3-8]. In comparison to ScN, YN is not as well investigated. Its ground state has a B1 (rock-salt) structure with a recently reported indirect band gap of 0.498 eV [9], in comparison to previously calculated theoretical values of 0.54-0.85 eV [10,11]. In contrast to the chemically-stable ScN, when subjected to moist air YN reacts and forms oxide-hydroxides YOOH [12], hence thin films of YN require a capping layer to avoid this effect [13]. With the exception of wurtzite $\text{Y}_x\text{In}_{1-x}\text{N}$ [9], Y has mostly been used in nitrides to phase-stabilize cubic Cr-Al-Y-N coatings [14,15] and to promote the oxidation resistance of Ti-Al-N hard coatings [16]. YN was also suggested as a buffer layer for GaN epilayers [17].

II. Experimental details

In this work *ab initio* calculations of the mixing enthalpies and lattice parameters of cubic (NaCl, B1), hexagonal layered (B_k) and wurtzite (B4) $\text{Y}_x\text{Al}_{1-x}\text{N}$ solid solutions were carried out within a density-functional theory (DFT) framework. The alloys were modeled at the compositions $x=0.125, 0.25, 0.375, 0.5, 0.625, 0.75, \text{ and } 0.875$ according to the special quasirandom structure (SQS) method [18] using 128 atoms supercells. In the case of cubic SQS-structures, only the internal positions were relaxed for each volume to find the equilibrium lattice spacings and zero-pressure enthalpies. For the layered hexagonal and wurtzite structures, the internal positions and the cell shapes were relaxed for every volume. These two structures were prepared with the same atomic positions in the SQS-supercells with the exceptions of a shift in the relative metal and nitrogen sublattices and different initial guesses of the c/a parameter: 1.1 for the B_k and 1.5 for the B4 structure. The projected augmented wave (PAW) method within the Vienna Ab-initio Simulation Package (VASP) [19-21] was used together with the Perdew, Burke, Ernzerhof generalized gradient approximation (PBE-GGA) as the exchange-correlation

functional [22]. A 3x3x3 Monkhorst-Pack [23] k-mesh and an energy cutoff of 400 eV were used in all calculations.

In parallel, ternary 300 nm thick $Y_xAl_{1-x}N$ films with $x=0, 0.04, 0.13, \text{ and } 0.22$ at heater temperatures of 500, 700, and 900 °C were prepared on $Al_2O_3(0001)$ and Si(100) substrates by magnetically unbalanced reactive DC magnetron sputtering in a mixed Ar/ N_2 plasma discharge in a UHV chamber [24] with a base pressure $<4 \times 10^{-6}$ Pa and a process pressure of 0.66 Pa. Two separate elemental targets: 75 mm diameter 99.9999% pure Al and 50 mm diameter 99.99% pure Y were used in a constant power mode. The relative amounts of Y and Al were controlled by the relative applied target power while keeping the total power at 350 W. During growth, -30 V dc substrate bias was applied. Thermal degassing at the selected growth temperature was performed for 1 h and the targets were clean-sputtered for 3 minutes in pure Ar and 3 minutes in Ar/ N_2 atmosphere prior to deposition. To avoid oxygen contamination, a 5 nm capping layer of AlN was deposited at room temperature at 1.33 Pa of N_2 and floating potential. Composition and impurity levels were determined by time of flight energy elastic recoil detection analysis (ToF-E ERDA) using a primary ion beam of 40 MeV $^{127}I^{9+}$ performed at the Tandem Laboratory in Uppsala, Sweden. X-ray diffraction (XRD) and X-ray reflectivity (XRR) measurements were done using X'pert Pro and Empyrean MRD diffractometers from PANalytical. Spectroscopic ellipsometry (SE) was performed using a Variable Angle J. A. Woollam ellipsometer. Data were collected at room temperature, in the 1-6.5 eV energy region with a step of 0.01 eV, at incidence angles of 65° and 75°. Transmission electron microscopy (TEM), high angle annular dark field HAADF-(S)TEM imaging, and (S)TEM-EDX elemental mapping were performed in the doubly corrected Linköping FEI Titan³ 60-300, operated at 300 kV. For the (S)TEM-EDX measurements, a ~ 3 Å electron probe was used.

III. Results and discussion

Figure 1 shows the calculated mixing enthalpies for wurtzite $Y_xAl_{1-x}N$ for $0 < x < 0.875$, cubic for $0 < x < 1$, and layered hexagonal for $0.5 < x < 1$. The mixing enthalpies are positive with respect to the parent binary systems (YN, AlN) for all three structures suggesting that alloying would result in a metastable material with an intrinsic driving force towards clustering and phase separation. It is noted that the wurtzite

phase is favored with respect to the cubic phase for Y content in the range $0 < x < 0.75$ and layered hexagonal phase in the range $0.5 < x < 0.875$. The crossing point between wurtzite and cubic phases occurs at higher Y content than what was obtained for Sc content of $x=0.6$ in $\text{Sc}_x\text{Al}_{1-x}\text{N}$ [25]. Comparing $\text{Y}_x\text{Al}_{1-x}\text{N}$ with the previously studied $\text{Sc}_x\text{Al}_{1-x}\text{N}$ system [25,26], the presented alloys display considerably higher mixing enthalpies. Since Sc and Y share a similar electronic bonding behaviour, the larger volume difference between YN and AlN as compared to that between ScN and AlN is likely to be the major contributor to this finding. Calculations of the mixing enthalpy for the B1 and B4 phases of YAlN have previously been done by Rovere *et al.* [15]. The differences are that we additionally consider the B_k phase which has a lower energy minimum compared to wurtzite in pure YN, and use larger supercells with a more accurate description of the configurational disorder between Y and Al. As a consequence, we find the crossing point where the cubic phase becomes lower than the wurtzite to be at a Y-content of $x=0.75$ while in Ref. [15] it was suggested to be as high as $x=0.875$.

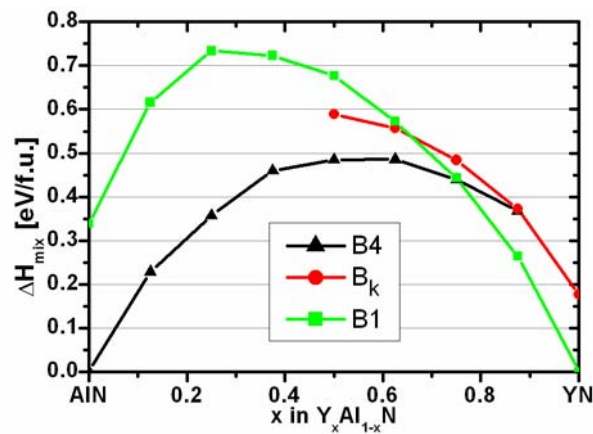


Figure 1. *Ab initio* calculated mixing enthalpies for wurtzite (B4), layered hexagonal (B_k), and cubic (B1) crystal structures for $0 \leq x \leq 1$ $\text{Y}_x\text{Al}_{1-x}\text{N}$.

ToF-E ERDA was performed on $\text{Y}_x\text{Al}_{1-x}\text{N}/\text{Si}$ samples. All samples are stoichiometric with $(\text{Al}+\text{Y})/\text{N}$ ratio being 1, levels of Y and Al being constant throughout the film with $x=0, 0.04, 0.13, \text{ and } 0.22$, with an accuracy of 3%. Below the initial surface oxide layer the samples contain 1-2 at.% O, 0.5 at.% F, and traces of C. For samples with $x=0.22$, trace amounts of Ar, W, and Fe are also seen. The O-rich surface layer is of similar thickness in all $\text{Y}_x\text{Al}_{1-x}\text{N}$ films. In general, the amount of contaminants is proportional to the Y fraction in the film; this suggests that the main sources of contaminations are the Y elemental target and Y acting as a getter for residual gasses in the chamber [17].

XRD $\theta/2\theta$ scan results for the $Y_xAl_{1-x}N$ samples deposited at $T=700\text{ }^\circ\text{C}$ are displayed in Figure 2 (a). At $x=0.04$ the 0002 peak intensity is comparable to the pure AlN ($x=0$) sample, but with increasing Y concentration the intensity is dropping and the peak position is shifting consistently towards lower 2θ values. No peaks corresponding to cubic YN were observed. The XRD peak intensity increased with increased growth temperature for all studied concentrations, results for $x=0.13$ grown at $T=700$ and $900\text{ }^\circ\text{C}$ are displayed in Figure 2 (b). Pole figure measurements (not shown) indicate a c-axis oriented film with an epitaxial relationship to the substrate in the case of $x\leq 0.13$ at $T=900\text{ }^\circ\text{C}$ and polycrystalline film in the case of $T=700\text{ }^\circ\text{C}$. The improved crystalline quality differs from our observations for the ScAlN thin films [6], where increased deposition temperature degraded the crystalline quality and resulted in a separation into ScN-rich and AlN-rich domains for samples grown at $T=800\text{ }^\circ\text{C}$. This suggests that the diffusivity of Y atoms is slower than Sc in or on AlN. While the increased growth temperature improves the Y mobility and promotes crystallization, $T=900\text{ }^\circ\text{C}$ is not enough for segregation of YN-rich domains with up to $x=0.22$.

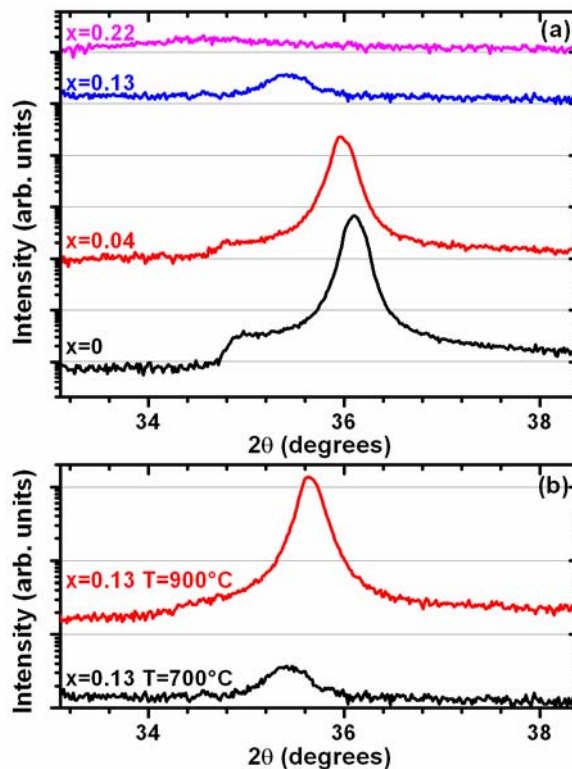


Figure 2. X-ray diffraction pattern on a logarithmic scale for (a) $Y_xAl_{1-x}N$ samples with $x=0, 0.04, 0.13,$ and 0.22 deposited at $T=700\text{ }^\circ\text{C}$, and (b) $x=0.13$ deposited at $T=700$ and $900\text{ }^\circ\text{C}$.

Results from the measurements of the lattice constants together with theoretical calculations are presented in Figure 3 (a) and (b). The ionic radius of Y is larger than Al, which can explain the increase in lattice constants with increased Y concentrations. The crystalline quality of samples with $x=0.22$ was not sufficient to get accurate experimental results. The small overestimation of the calculated lattice parameters as compared to the measured values is a well-known effect of the PBE-GGA functional [27]. However, the shift is small and the c/a ratio, linearly interpolated between the considered compositions $x=0.00$, $x=0.125$, and $x=0.25$, corresponds well to the experimental data, summarized in Table 1. The consistency between calculated and measured lattice spacings, and their change with composition confirms the formation of solid solutions.

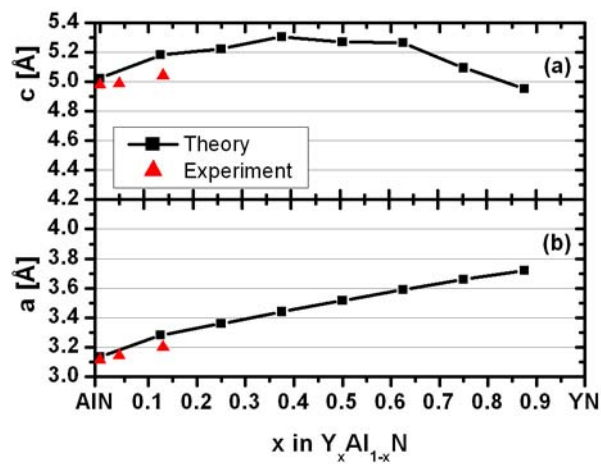


Figure 3. *Ab initio* calculated (black line+square) and experimentally obtained (red triangle) lattice constants (a) c , (b) a for the wurtzite structure $Y_xAl_{1-x}N$. The lines are guides for the eye.

Cross sectional samples with $x=0.13$ grown at $T=700$ and 900 °C were investigated by (S)TEM. STEM imaging of the films reveal a columnar appearance (Figure 4 (a) and (b)). STEM-EDX elemental mapping across the columns revealed no segregation into Al- and Y-rich domains (not shown). Dark field (DF) TEM show a fine columnar microstructure near the substrate interface which coarsens with film thickness in the $T=700$ °C sample. For the increased growth temperature, the fine features extend further into the film, with eventual coarsening (Figure 4 (c) and (d)). Selected area electron diffraction (SAED) patterns exhibit arc-like features for the $T=700$ °C sample indicating a polycrystalline material with slight variations in orientation (Figure 4 (e)). By increasing the growth temperature to $T=900$ °C the SAED pattern exhibit nearly discrete diffraction spots and an alignment of the c -axis with the

growth direction (Figure 4 (f)). Nanodiffraction experiments (not shown) for the samples deposited at $T=700\text{ }^{\circ}\text{C}$ reveal no changes in the diffraction pattern going from the interface towards the top of the film, while for $T=900\text{ }^{\circ}\text{C}$ diffraction spots are sharper closer to the interface. HRTEM imaging reveals that the fine features are all (0001) oriented, but azimuthally twisted with respect to each other. Forming these fine structures is a way for the film material to relax into a metastable state. Apparently, with increasing film thickness, this further relaxes into the columnar polycrystalline structure.

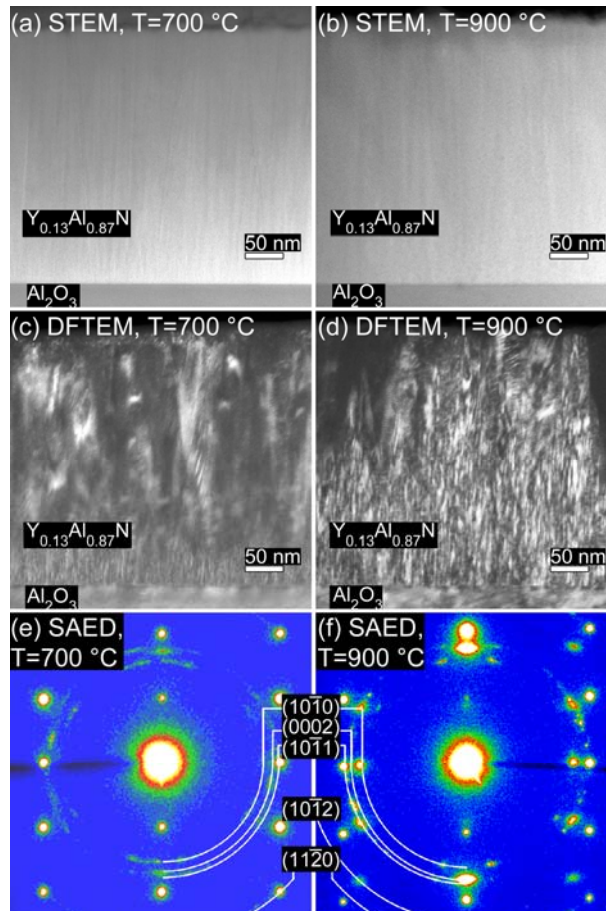


Figure 4. Cross-sectional STEM, dark field TEM and SAED images of $\text{Y}_{0.13}\text{Al}_{0.87}\text{N}$ thin films deposited at $700\text{ }^{\circ}\text{C}$: (a), (c), (e), and $900\text{ }^{\circ}\text{C}$: (b), (d), and (f), respectively.

The ellipsometry data of the $\text{Y}_x\text{Al}_{1-x}\text{N}/\text{Si}$ samples deposited at $700\text{ }^{\circ}\text{C}$ were analyzed using a layered model and the $\text{Y}_x\text{Al}_{1-x}\text{N}$ film was parametrized using a standard dielectric function model with a Cauchy term and a Lorentzian oscillator, more details can be found elsewhere[28]. The data analysis renders the complex dielectric function of $\text{Y}_x\text{Al}_{1-x}\text{N}$ and the band gap energy of the $\text{Y}_x\text{Al}_{1-x}\text{N}$ is then extracted from the Lorentzian energy position. The extracted value of the AlN band gap is 6.2 eV , which is in excellent agreement with values for high-quality single-crystal material [29]. The analysis indicates that the band

gap of $Y_xAl_{1-x}N$ is direct for the studied compositional range and the results are presented in Figure 5 and Table 1. The band gap energy of $Y_xAl_{1-x}N$ decreases with increasing Y composition as expected for a solid solution. Our electronic structure calculations confirm that Y-addition introduces states in the band gap of w-AlN, decreasing its value while still preserving the overall semiconducting character. However, due to well-known underestimations of band gaps in standard DFT approximations, further investigations are needed for a quantitative theoretical analysis.

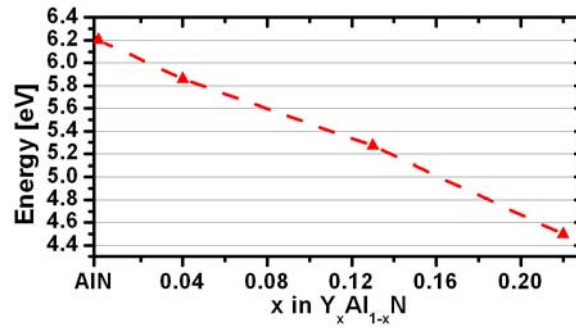


Figure 5. $Y_xAl_{1-x}N$ direct band gap energies (red triangle) determined from the SE analysis for Y content $x=0, 0.04, 0.13,$ and 0.22 . The dashed line is a guide for the eye.

Table 1. Direct band gap E_g , measured lattice constants a_{exp} and c_{exp} , experimental $(c/a)_{exp}$ and linear interpolation between theoretical $(c/a)_{calc}$ at $x=0, 0.125,$ and 0.25 , for $Y_xAl_{1-x}N$ thin films.

x in $Y_xAl_{1-x}N$	E_g (eV)	c_{exp} (Å)	a_{exp} (Å)	$(c/a)_{exp}$	$(c/a)_{calc}$
0	6.2	4.98	3.11	1.60	1.63
0.04	5.9	4.99	3.14	1.59	1.6
0.13	5.3	5.04	3.20	1.57	1.58
0.22	4.5				

IV. Conclusions

In conclusion, polycrystalline c -axis oriented wurtzite structure $Y_xAl_{1-x}N$ thin films with $x=0, 0.04, 0.13,$ and 0.22 can be deposited using reactive magnetron co-sputtering from elemental Al and Y targets in Ar/ N_2 discharge. Calculations show large positive mixing enthalpies for all investigated phases, wurtzite being the lowest for $0 < x < 0.75$. The compositional homogeneity of films with linear increase in lattice constants with x supports a solid solution, attributed to the quenched diffusion of Y. Experimentally determined lattice constants match well with theoretical predictions. The crystalline quality of the films

is, however, degrading with increasing concentration of Y. Increasing the growth temperature improves the crystalline quality due to higher adatom mobility. Optical characterization confirms a solid solution and suggests $Y_xAl_{1-x}N$ to be a direct band gap semiconductor with $E_g=4.5$ eV at $x=0.22$.

Acknowledgements

We acknowledge the financial support by the Linköping Linnaeus Initiative on Nanoscale Functional Materials (LiLiNFM) supported by the Swedish Research Council (VR) under grant No.349-2008-6582. The ERDA measurements were performed by Dr. Jens Jensen from Linköping University using the Tandem Laboratory at Uppsala University, Sweden. Nebiha Ben Sedrine acknowledges FCT Portugal under SFRH/BPD/66818/2009 and Vanya Darakchieva acknowledges support from VR under grant No.2010-3848 and the Swedish Governmental Agency for Innovation Systems (VINNOVA) under grant No.2011-03486. The calculations were carried out using supercomputer resources provided by the Swedish national infrastructure for computing (SNIC) at the PDC center for high performance computing.

Figure and table captions

Figure 1. *Ab initio* calculated mixing enthalpies for wurtzite (B4), layered hexagonal (B_k), and cubic (B1) crystal structures for $0 \leq x \leq 1$ $Y_xAl_{1-x}N$.

Figure 2. X-ray diffraction pattern on a logarithmic scale for (a) $Y_xAl_{1-x}N$ samples with $x=0, 0.04, 0.13,$ and 0.22 deposited at $T=700$ °C, and (b) $x=0.13$ deposited at $T=700$ and 900 °C.

Figure 3. *Ab initio* calculated (black line+square) and experimentally obtained (red triangle) lattice constants (a) c , (b) a for the wurtzite structure $Y_xAl_{1-x}N$. The lines are guides for the eye.

Figure 4. Cross-sectional STEM, dark field TEM and SAED images of $Y_{0.13}Al_{0.87}N$ thin films deposited at 700 °C: (a), (c), (e), and 900 °C: (b), (d), and (f), respectively.

Figure 5. $Y_xAl_{1-x}N$ direct band gap energies (red triangle) determined from the SE analysis for Y content $x=0, 0.04, 0.13,$ and 0.22 . The dashed line is a guide for the eye.

Table 1. Direct band gap E_g , measured lattice constants a_{exp} and c_{exp} , experimental $(c/a)_{exp}$ and linear interpolation between theoretical $(c/a)_{calc}$ at $x=0, 0.125,$ and 0.25 , for $Y_xAl_{1-x}N$ thin films.

References

- [1] Schuster J C and Bauer J 1985 The ternary systems ScAlN and YAlN *Journal of the Less-Common Metals* **109** (2) 345-350.
- [2] Bernardini F, Fiorentini V and Vanderbilt D 1997 Spontaneous polarization and piezoelectric constants of III-V nitrides *Physical Review B - Condensed Matter and Materials Physics* **56** (16) R10024-R10027.
- [3] Akiyama M, Kamohara T, Kano K, Teshigahara A, Takeuchi Y and Kawahara N 2009 Enhancement of piezoelectric response in scandium aluminum nitride alloy thin films prepared by dual reactive cosputtering *Adv Mater* **21** (5) 593-596.
- [4] Tasnádi F, Alling B, Höglund C, Wingqvist G, Birch J, Hultman L and Abrikosov I A 2010 Origin of the anomalous piezoelectric response in wurtzite $\text{Sc}_x\text{Al}_{1-x}\text{N}$ alloys *Phys Rev Lett* **104** (13) 137601.
- [5] Wingqvist G, Tasnádi F, Zukauskaitė A, Birch J, Arwin H and Hultman L 2010 Increased electromechanical coupling in w- $\text{Sc}_x\text{Al}_{1-x}\text{N}$ *Appl Phys Lett* **97** (11) 112902.
- [6] Zukauskaitė A, Wingqvist G, Palisaitis J, Jensen J, Persson P O Å, Matloub R, Murali P, Kim Y, Birch J and Hultman L 2012 Microstructure and dielectric properties of piezoelectric magnetron sputtered w- $\text{Sc}_x\text{Al}_{1-x}\text{N}$ thin films *J Appl Phys* **111** (9) 093527.
- [7] Matloub R, Artieda A, Sandu C, Milyutin E and Murali P 2011 Electromechanical properties of $\text{Al}_{0.9}\text{Sc}_{0.1}\text{N}$ thin films evaluated at 2.5 GHz film bulk acoustic resonators *Appl Phys Lett* **99** (9) 092903.
- [8] Moreira M, Bjurström J, Katardjev I and Yantchev V 2011 Aluminum scandium nitride thin-film bulk acoustic resonators for wide band applications *Vacuum* **86** (1) 23-26.
- [9] Zoita C N, Braic M and Braic V 2011 Structural, optical and electronic properties of $\text{In}_{1-x}\text{Y}_x\text{N}$ thin films *Dig J Nanomat Biostr* **6** (4) 1877-1886.
- [10] Lü T and Huang M 2007 Electronic structure of ScN and YN: Density-functional theory LDA and GW approximation calculations *Chin Phys* **16** (1) 62-66.
- [11] Stampfl C, Mannstadt W, Asahi R and Freeman A J 2001 Electronic structure and physical properties of early transition metal mononitrides: Density-functional theory LDA, GGA, and screened-exchange LDA FLAPW calculations *Phys Rev B Condens Matter Mater Phys* **63** (15) 1551061-15510611.
- [12] Dismukes J P, Yim W M, Tietjen J J and Novak R E 1970 Vapor deposition of semiconducting mononitrides of scandium, yttrium, and the rare- earth elements *R.C.A.Review* **31** (4) 680-691.
- [13] Gregoire J M, Kirby S D, Scopelianos G E, Lee F H and Van Dover R B 2008 High mobility single crystalline ScN and single-orientation epitaxial YN on sapphire via magnetron sputtering *J Appl Phys* **104** (7) 074913.
- [14] Rovere F and Mayrhofer P H 2007 Impact of yttrium on structure and mechanical properties of Cr-Al-N thin films *J Vac Sci Technol A Vac Surf Films* **25** (5) 1336-1340.

- [15] Rovere F, Music D, Schneider J M and Mayrhofer P H 2010 Experimental and computational study on the effect of yttrium on the phase stability of sputtered Cr–Al–Y–N hard coatings *Acta Materialia* **58** (7) 2708-2715.
- [16] Lembke M I, Lewis D B, Münz W D and Titchmarsh J M 2001 Significance of Y and Cr in TiAlN hard coatings for dry high speed cutting *Surf Eng* **17** (2) 153-158.
- [17] De La Cruz W, Díaz J A, Mancera L, Takeuchi N and Soto G 2003 Yttrium nitride thin films grown by reactive laser ablation *J Phys Chem Solids* **64** (11) 2273-2279.
- [18] Zunger A, Wei S -, Ferreira L G and Bernard J E 1990 Special quasirandom structures *Phys Rev Lett* **65** (3) 353-356.
- [19] Blöchl P E 1994 Projector augmented-wave method *Physical Review B* **50** (24) 17953-17979.
- [20] Kresse G and Hafner J 1993 Ab initio molecular dynamics for open-shell transition metals *Physical Review B* **48** (17) 13115-13118.
- [21] Kresse G and Furthmüller J 1996 Efficiency of ab-initio total energy calculations for metals and semiconductors using a plane-wave basis set *Computational Materials Science* **6** (1) 15-50.
- [22] Perdew J P, Burke K and Ernzerhof M 1996 Generalized gradient approximation made simple *Phys Rev Lett* **77** (18) 3865-3868.
- [23] Monkhorst H J and Pack J D 1976 Special points for Brillouin-zone integrations *Physical Review B* **13** (12) 5188-5192.
- [24] Seppänen T, Persson P O Å, Hultman L, Birch J and Radnóczy G Z 2005 Magnetron sputter epitaxy of wurtzite $\text{Al}_{1-x}\text{In}_x\text{N}$ ($0.1 < x < 0.9$) by dual reactive dc magnetron sputter deposition *J Appl Phys* **97** (8) 1-9.
- [25] Höglund C, Birch J, Alling B, Bareño J, Czigány Z, Persson P O Å, Wingqvist G, Zukauskaitė A and Hultman L 2010 Wurtzite structure $\text{Sc}_{1-x}\text{Al}_x\text{N}$ solid solution films grown by reactive magnetron sputter epitaxy: Structural characterization and first-principles calculations *J Appl Phys* **107** (12) 123515.
- [26] Höglund C, Bareño J, Birch J, Alling B, Czigány Z and Hultman L 2009 Cubic $\text{Sc}_{1-x}\text{Al}_x\text{N}$ solid solution thin films deposited by reactive magnetron sputter epitaxy onto ScN(111) *J Appl Phys* **105** (11) 113517.
- [27] Haas P, Tran F and Blaha P 2009 Calculation of the lattice constant of solids with semilocal functionals *Physical Review B - Condensed Matter and Materials Physics* **79** (8) 085104.
- [28] Ben Sedrine N, Zukauskaitė A, Birch J, Hultman L and Darakchieva V 2012 *In Manuscript*.
- [29] Vurgaftman I, Meyer J R and Ram-Mohan L R 2001 Band parameters for III-V compound semiconductors and their alloys *J Appl Phys* **89** (11 I) 5815-5875.